Spatial heterogeneity of intracellular Ca^{2+} signals in axons of basket cells from rat cerebellar slices

Isabel Llano, Yusuf P. Tan and Carlo Caputo

Arbeitsgruppe Zelluläre Neurobiologie, Max-Planck-Institut für Biophysikalische Chemie, am Fassberg, D-37070 Göttingen, Germany

1. Using tight-seal whole-cell recording and digital fluorescence imaging, we studied intracellular calcium (Ca_i^{2+}) dynamics in cerebellar basket cells, whose dendrites, axon and presynaptic terminals are coplanar, an optimal configuration for simultaneous optical measurements of all functional domains.
2. In Cs^+-loaded neurones, depolarizing pulses induced large Ca_i^{2+} transients in single axonal varicosities and synaptic terminals, contrasting with much weaker signals between varicosities or in the somato-dendritic domain.
3. Axonal branch points consistently displayed $[Ca^{2+}]_i$ rises of similar magnitude and time course to those in axonal terminals and varicosities.
4. In biocytin-filled basket cells, varicosity-like swellings were present along the axon including its branch points. Thus, axonal enlargements are not due to fluorescence-induced cell damage.
5. The spatial heterogeneity of Ca_i^{2+} signals was also observed in K^+-loaded cells upon depolarizing trains, suggesting that this behaviour is an intrinsic property of Ca_i^{2+} homeostasis in basket cells.
6. We conclude that depolarization of basket cell axons evokes high local Ca_i^{2+} signals in synaptic terminals, *en passant* varicosities and branch points. While high $[Ca^{2+}]_i$ in presynaptic structures presumably triggers transmitter release, Ca_i^{2+} transients at branch points may control signal transmission in the axonal arborization.

Since the pioneering work of Katz & Miledi (1967) changes in the intracellular Ca^{2+} concentration in presynaptic terminals have been considered as one of the crucial steps of excitation–secretion coupling. Highly localized sites of Ca^{2+} entry have been demonstrated at the giant presynaptic terminal of the squid stellate ganglion, where $[Ca^{2+}]_i$ reaches levels in the hundreds of micromolar range close to release sites during exocytosis (Simon & Llinás, 1985; Llinás, Sugimori & Silver, 1992). High $[Ca^{2+}]_i$ rises are also a requisite for exocytosis in retinal bipolar cell terminals (Heidelberger, Heinemann, Neher & Matthews, 1994). In recent years considerable progress has been achieved in the measurement of Ca_i^{2+} concentrations in neuronal dendrites (reviewed by Regehr & Tank, 1994) and the role of Ca_i^{2+} in postsynaptic information processing (reviewed by Yuste & Tank, 1996). However, geometric constraints have so far limited studies of presynaptic Ca_i^{2+} dynamics in single terminals of mammalian neurones to a few preparations with unusually large terminals, namely the mossy fibre terminals in the hippocampus (Regehr & Tank, 1991) and the calyces of Held of the trapezoid body (Borst, Helmchen & Sakmann, 1995). Recently, a study in single axons of cultured cortical neurones has been reported, demonstrating that action potentials are reliably transmitted to release sites, thus eliminating signal propagation as a major source of variability at the glutamatergic synapses formed by these neurones (Mackenzie, Umemiya & Murphy, 1996). Further studies on axonal Ca_i^{2+} dynamics with subcellular resolution in mammalian brain slices are essential to understand the basic principles governing synaptic transmission in the central nervous system as well as short- and long-term changes in synaptic efficacy. Progress in this area is particularly desirable in view of recent work using fluorescence measurements from populations of neurones, which show that elevations in axonal Ca_i^{2+} play different roles in the induction and maintenance of long- (Regehr & Tank, 1991) and short-term synaptic plasticity (Regehr, Delaney & Tank, 1994; Wu & Saggau, 1994*a*).

In the cerebellar cortex, information processing is critically regulated by the inhibition exerted by interneurones onto the principal cells of the circuit, the Purkinje cells (Eccles, Llinás & Sasaki, 1966; Armstrong & Rawson, 1979; O'Donoghue, King & Bishop, 1989). The GABAergic synapses between interneurones and Purkinje cells are characterized by large fluctuations in the amplitude of the inhibitory postsynaptic currents (IPSCs) contributed by a single interneurone (Vincent & Marty, 1996). These inhibitory synapses are subject to short- and long-term modifications triggered by

$[Ca^{2+}]_i$ rises in the postsynaptic cell (Llano, Leresche & Marty 1991; Kano, Rexhausen, Dreessen & Konnerth, 1992; Vincent, Armstrong & Marty, 1992; Vincent & Marty, 1993) and by alterations in the presynaptic levels of cAMP (Llano & Gerschenfeld, 1993). In the present work we studied Ca^{2+}-dependent fluorescence transients in cerebellar basket cells. The dendrites, axon and presynaptic terminals of these interneurones are contained in the sagittal plane, facilitating simultaneous optical measurements of all the subregions of a single cell. We found that depolarization-induced Ca_i^{2+} transients in basket cells have a marked spatial heterogeneity, being much larger in discrete spots of the axon and its terminals than in dendrites and soma.

METHODS

Experiments were done at 20–23 °C in interneurones located in the lowest third of the molecular layer of the cerebellar cortex. Following Ramón y Cajal's (1911) classification, these neurones are considered basket cells. Sagittal cerebellar slices (180 μm thick) were prepared, as previously described (Llano, Marty, Armstrong & Konnerth, 1991), from rats aged 13–16 days that had been decapitated following cervical dislocation. Slices were perfused (1·5 ml min^{-1}) with a saline containing (mM): 125 NaCl, 2·5 KCl, 1·25 NaH_2PO_4, 26 $NaHCO_3$, 2 $CaCl_2$, 1 $MgCl_2$, and 10 glucose, equilibrated with a 95% O_2–5% CO_2 mixture (pH 7·3). Tight-seal whole-cell recordings were performed with pipettes (2·5–3·5 MΩ) filled with a solution containing (mM): 150 CsCl, 4·6 $MgCl_2$, 10 Hepes-Cs, 0·4 Na-GTP, 4 Na-ATP (pH 7·3). In some experiments K^+ replaced Cs^+ as the main cation. Intracellular solutions were supplemented with 200 μM of the Ca^{2+}-sensitive probe Calcium Green-5N (CG5N; Molecular Probes, Eugene, OR, USA). This dye was chosen after preliminary tests with several other Ca^{2+}-sensitive indicators in view of the following considerations. (i) It has a low molecular weight and a correspondingly high diffusion coefficient. (ii) It has a high quantum efficiency. (iii) It has a low affinity for Ca^{2+} (see below); this is important to avoid dye saturation and exogenous buffer effects (Neher & Augustine, 1992), and to obtain an accurate estimate of the time course of Ca_i^{2+} decay. (iv) We found that under the high illumination intensities used in our experiments CG5N had significantly less bleaching than fura-2 or fluo-3 and less phototoxic effects than other indicators of the Calcium Green series. Even with CG5N some photodamage eventually occurred, as testified by an increase in the holding current. The collection of data was discontinued as soon as the value of this current reached −70 pA at a holding potential of −60 mV.

Digital fluorescence images were obtained using a Zeiss Axioskop microscope (×63 water-immersion lens; numerical aperture, 0·9) equipped with an image acquisition system and a monochromatic light source for fluorescence excitation (T.I.L.L. Photonics, Planegg, Germany). A detailed description of this system can be found in Messler, Harz & Uhl (1996). Briefly, the output of a 75 W xenon lamp is focused on a scanning monochromator and coupled to the microscope by a quartz fibre and an appropriate lens. At 488 nm, the illumination intensity at the back aperture of the objective amounts to 1 mW. The dichroic mirror and high-pass emission filter used in the present work had centre wavelengths at 505 and 507 nm, respectively. Images were acquired with a peltier-cooled slow scan CCD camera (Thompson 7863 frame transfer chip; 384 pixels by 286 pixels; pixel size 0·36 μm after ×63 magnification) connected to a 12-bit A/D converter. The large dynamic range of the recording system ensured that saturation did not occur in the present work, even in the soma where the basal counts were 10-fold larger than in neurites.

The standard protocol to study Ca_i^{2+} transients consisted of acquiring a sequence of sixteen to twenty images with an integration time of 70 or 100 ms, and 6 or 3 ms intervals between consecutive images. Image acquisition was started while the cell was held at −60 mV and a single depolarizing voltage step was applied at the end of the fourth image. Figure 1*A* shows typical membrane currents due to the activation of voltage-gated Na^+ and Ca^{2+} channels, elicited by a 50 ms pulse to 0 mV. Fluorescence changes associated with this type of stimuli were analysed off-line by measuring the average fluorescence in small 'regions of interest' (ROIs; 6–8 pixels, corresponding to 0·8–1·1 μm^2). The average fluorescence in each ROI was then converted to the percentage change in fluorescence: $\Delta F/F_0 = 100(F - F_r)/(F_r - B)$, where F is the measured fluorescence signal at any given time, F_r is the average fluorescence from four consecutive images preceding the voltage step, B is the average value of the background fluorescence from five regions located in the periphery of the visual field and of equal size to the cellular ROIs, and $F_0 = F_r - B$. Figure 1*B* plots the raw fluorescence data (counts) for two axonal ROIs and the mean B value, as a function of time; the arrow marks the onset of the pulse which elicited the current shown in Fig. 1*A*. As in this example, background values were stable during each experimental run and the basal counts in the various ROIs analysed were unambiguously distinguishable from the background. Thus, in eleven cells, for 70 ms integrations the mean ± S.E.M. for the background counts was 23·3 ± 2·7; the corresponding value for the pre-stimuli counts in axonal ROIs was 39·6 ± 3·5 and the ratio of pre-stimuli axonal counts to B counts was 1·8 ± 0·12. The plot in Fig. 1*C* shows the result of conversion of the data from Fig. 1*B* to $\Delta F/F_0$. Note that there is a significant difference between the peak values reached at the two axonal spots, although they had similar levels of basal counts.

It can be shown that the ratio of $\Delta F/F_0$ depends only on changes in Ca_i^{2+} and not on variables such as optical filtering, dye concentration or focus position. We call the ideal fluorescence and the measured fluorescence at a given point of co-ordinates (x,y,z) as $f(x,y,z)$ and $F(x,y,z)$, respectively. The two functions are related to each other by the equation:

$$F(x,y,z) = B + \iiint f(u,v,w) \times \mathrm{psf}(x-u,\ y-v,\ z-w)\mathrm{d}u\mathrm{d}v\mathrm{d}w,$$

where psf corresponds to the point spread function of the optical system. If it is assumed that the Ca^{2+} concentration is homogeneous, it follows that (i) $f(u,v,w)$ is zero out of the fluorescent volume and (ii) it is a function of the Ca^{2+} concentration ($\phi([Ca^{2+}]_i)$) in that volume. Then,

$$F(x,y,z) = B + \iiint_V \phi([Ca^{2+}]_i) \times \mathrm{psf}(x-u, y-v, z-w)\mathrm{d}u\mathrm{d}v\mathrm{d}w,$$

$$F(x,y,z) - B = \phi([Ca^{2+}]_i)\iiint_V \mathrm{psf}(x-u, y-v, z-w)\mathrm{d}u\mathrm{d}v\mathrm{d}w,$$

where the integration is now carried out only in the volume, V, of the cell. The ratio of fluorescence measured after a stimulus (F_s) to the resting fluorescence (F_r) is therefore related only to the change in Ca^{2+} concentration:

$$(F_s - B)/(F_r - B) = \phi([Ca^{2+}]_i)_s/\phi([Ca^{2+}]_i)_r,$$

so that

$$\Delta F/F_0 = \phi([Ca^{2+}]_i)_s/\phi([Ca^{2+}]_i)_r - 1, \quad (1)$$

where $\phi([Ca^{2+}]_i)_s$ and $\phi([Ca^{2+}])_r$ correspond to the Ca^{2+} concentrations after a stimulus and at rest, respectively.

Two types of pseudocolour digital fluorescence images are shown in the Results section. Firstly, original pre- and post-stimuli images are shown. These correspond to the raw data (i.e. no subtraction of background counts, averaging or masking has been performed). They are displayed with a pseudocolour scale such that axonal fluorescent signals are clearly apparent, while signals in the soma and some of the largest dendritic spots are saturated. Secondly, images corresponding to $\Delta F/F_0$ are shown. For the preparation of the latter, masking and median filtering procedures were used to reduce the impulsive (so called 'salt and pepper') noise inherent to the calculation of ratio images. A three-step procedure was followed. (i) Generation of the F_0 image: four pre-pulse images were averaged and the mean value of the background (B, the value used for calculations of $\Delta F/F_0$ in ROIs from raw images) was subtracted from them. Whenever the subtraction yielded a negative value, the pixel value was set to 1 to avoid division by 0 or negative intensities. (ii) Generation of ΔF images: the F_0 image was subtracted from the post-stimuli images pixel by pixel; any pixel with a value less than 3 times the standard deviation of B was arbitrarily set to 0. (iii) Generation of $\Delta F/F_0$ images: each ΔF image was divided by the F_0 image, pixel by pixel; a median filter was applied to remove the remaining 'salt and pepper' noise, namely a 3×3 window slides along the image and the median intensity value of the pixels within the window becomes the value of the central pixel processed. This filter smoothes out the image slightly.

To obtain a rough estimate of the magnitude of the Ca_i^{2+} transients measured with CG5N, we performed calibrations of the recording system using a 400 μm internal diameter glass capillary sequentially perfused with a series of solutions of known Ca^{2+} concentration, ranging from 0 to 1 mM (calcium calibration kits nos 2 and 3 from Molecular Probes). The solutions contained 5 μM CG5N. Images were taken for each solution, and the counts from a small ROI at the centre of the capillary were plotted against the Ca^{2+} concentration. The resulting plot yielded an estimate for the K_d of CG5N for Ca^{2+} of ~20 μM. This value is higher than that reported by Molecular Probes (14 μM; Haugland, 1996) and lower than the estimates of 45 and 63 μM given by Escobar, Monck, Fernandez & Vergara (1994) and Zhao, Hollingworth & Baylor (1996), respectively. The different experimental procedures (cuvette measurements in Escobar *et al.*; absorbance measurements in Zhao *et al.*) may account for the widespread values. It should also be kept in mind that the apparent K_d in a cellular environment may differ from these values, since factors such as intracellular viscosity and binding to cytoplasmic components can influence the quantum efficiency of the dye. In skeletal muscle fibres, the cytoplasmic $[Ca^{2+}]_i$ changes obtained with CG5N have a slight delay and a larger half-width than those measured with other low affinity Ca^{2+} indicators such as furaptra; the slowness of the CG5N signal was interpreted as resulting from binding between the dye molecules and myoplasmic proteins which may alter the forward and/or

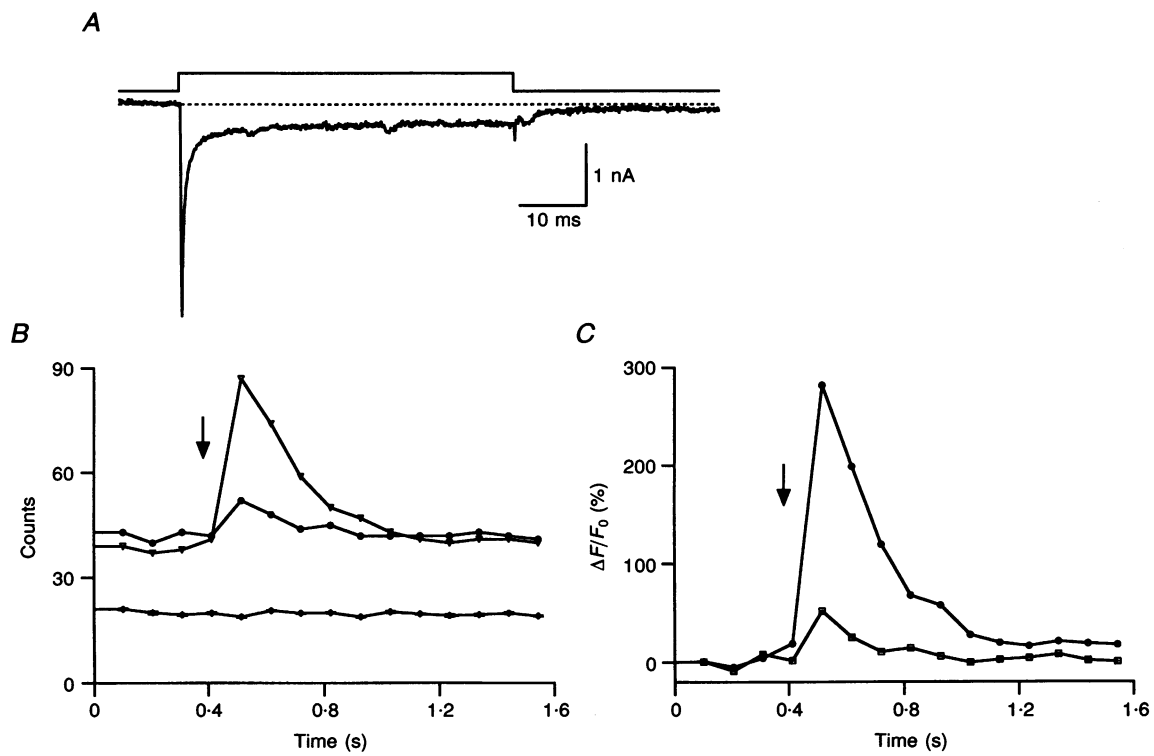

Figure 1. Experimental protocol to study Ca_i^{2+} signalling

A, membrane currents elicited in a CsCl-dialysed basket cell by a 50 ms depolarization to 0 mV, from a holding potential of −60 mV. The *P*/4 procedure was used to subtract capacitive and leak currents. *B*, plot, as a function of time, of the raw fluorescence data (counts) for two axonal regions of interest (ROIs: ▽ and ○), and for the mean value calculated from 5 background ROIs in the same visual field (●; the graph contains the S.E.M., but its value is smaller than the symbol size). *C*, plot of $\Delta F/F_0$ as a function of time for the two axonal ROIs in *B*. This experiment was performed in the same cell for which a pseudocolour image and $\Delta F/F_0$ plots are shown in Fig. 3. The ROI identified in *C* with the symbol ○ corresponds to the axonal terminal ROI identified with the symbol ▽ in Fig. 3*B*. The axonal ROI identified in *C* with the symbol □ corresponds to the ROI in the initial segment of the axon, identified with the symbol ○ in Fig. 3*C*.

backward rate constants of the reaction between CG5N and Ca^{2+} (Zhao *et al.* 1996). This problem may be particularly serious in muscle fibres, due to the large concentration of high-affinity Ca^{2+}-binding cytoplasmic proteins. Nonetheless, caution must be exercised when analysing with CG5N fast Ca_i^{2+} signals. However, the 26 ms difference in half-width of ΔF transients found between CG5N and furaptra (see Table 2 of Zhao *et al.* 1996) is unlikely to affect our results, for the signals studied in the present work are at least one order of magnitude slower (half-times of decay in the range of 370 ms) than those in skeletal muscle fibres.

For morphological characterization, non-superficial basket cells (i.e. located at least one cell layer deep in the slice) were chosen. They were loaded via patch pipettes with an intracellular solution containing (mM): 120 KCl, 10 EGTA, 1 $CaCl_2$, 4·6 $MgCl_2$, 10 Hepes-Cs, 0·4 Na-GTP, 4 Na-ATP (pH 7·3) and 0·2% (v/v) biocytin. Cells were maintained for ~15 min in whole-cell recording and subsequently processed for histological examination following the procedure described by Horikawa & Armstrong (1988) with an additional step for nickel enhancement. Stained cells were viewed in an upright microscope with ×63 and ×100 oil-immersion lenses. Photographs of sequential fields of view were scanned and photomontages were prepared using Adobe Photoshop software.

RESULTS

Heterogeneous Ca_i^{2+} signals in basket cells following somatic depolarization

Figure 2 illustrates the pattern of fluorescence reported by the Ca^{2+}-sensitive dye CG5N in a Cs^+-filled cerebellar basket cell at rest (*A*) and after a 100 ms long depolarizing voltage pulse (*B*). The ratio image ($\Delta F/F_0$; see Methods) is shown in *C* while *D* presents a light-transmitted image of the same portion of the slice. The Purkinje cell layer is roughly vertical, at one-third from the left border of the images, and

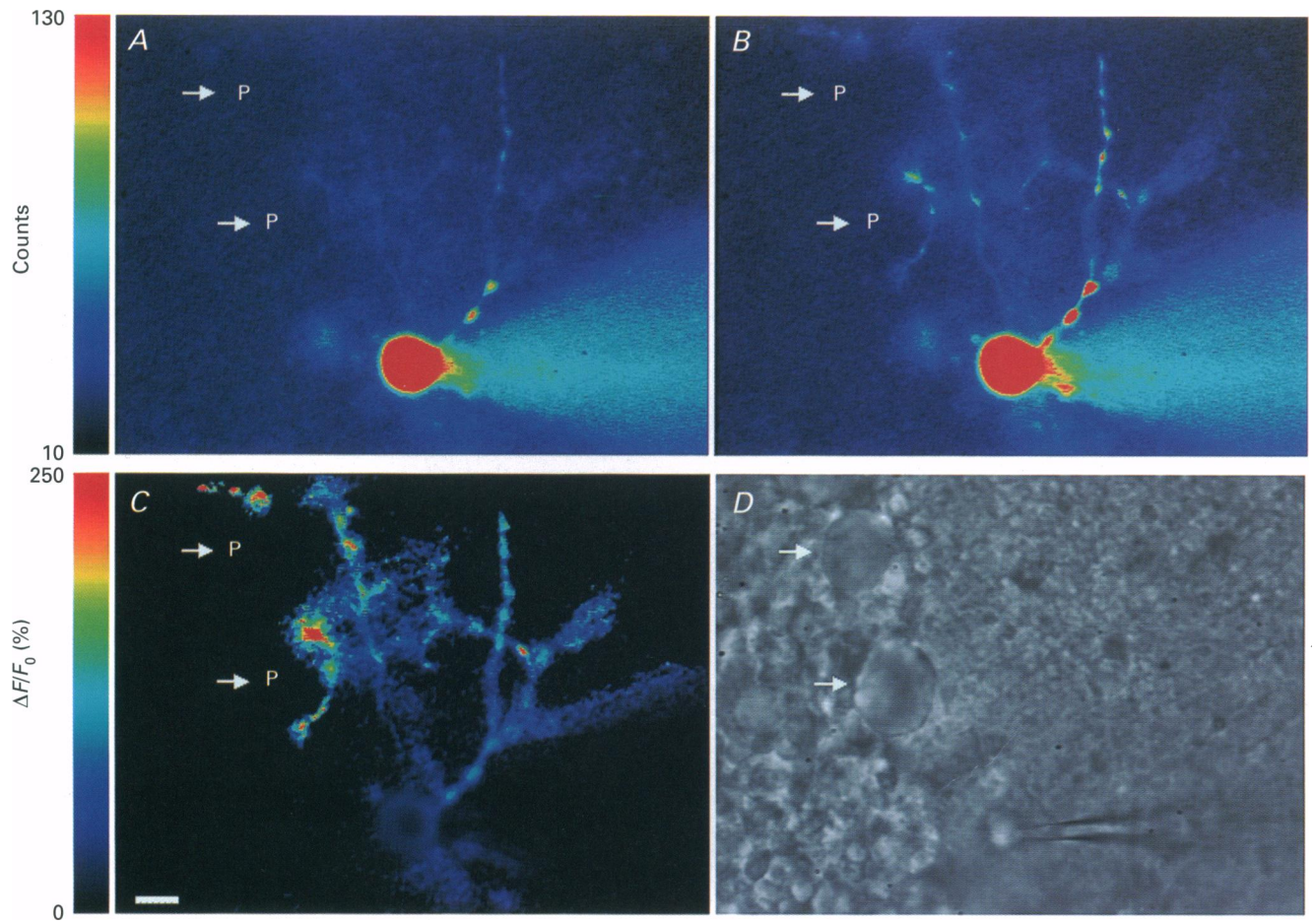

Figure 2. Ca_i^{2+} signalling in axon and dendrites of a cerebellar basket cell

A and *B*, pseudocolour images of the CG5N Ca^{2+}-dependent fluorescence at a holding potential of −60 mV at rest (*A*) and 29–129 ms after the end of a 100 ms pulse to 0 mV (*B*). *C*, $\Delta F/F_0$ image generated, as detailed in Methods, from the image shown in *B* and the average of 4 pre-stimulus images. *D*, light-transmitted image of the same portion of the slice. Depolarization-evoked changes in fluorescence are observed in different regions of the axon (neurite in the left half-field) and dendrite (neurite in the right half-field). For *A* and *B*, exposure was 100 ms; black to red indicates lowest to highest fluorescence. In this and the following figures, the pseudocolour images are displayed with a scale such that axonal fluorescent signals are clearly apparent, while signals in the soma and some of the largest dendritic spots are saturated. However, the original data was not saturated, as images were acquired with a sufficient dynamic range (see Methods). Scale bar in *C*, 10 μm.

the granule cell layer is on the left. The arrows in *D* point to somata of two Purkinje cells. Their position is identified by P in *A*, *B* and *C*, to illustrate co-localization with fluorescent spots at presumptive synaptic terminals. It is immediately apparent that the depolarization results in marked increases in fluorescence in selected areas of the neurone, indicating sharply localized changes in the intracellular Ca^{2+} concentration. Ca_i^{2+} changes are directly related to the ratio of the increase in fluorescence over the resting level ($\Delta F/F_0$). Figure 3*B*, *C* and *D* shows the time course of $\Delta F/F_0$ signals for selected regions of 1 μm^2 drawn in the expanded image of Fig. 3*A* (see Methods). In this example the peak value of the pulse-evoked $\Delta F/F_0$ was about 18% in the soma and 130% in the dendrites. Peak $\Delta F/F_0$ values along the dendrites were quite homogeneous, even though the resting fluorescence (F_0) varied along the length of the dendrites presumably due to local swellings. The largest of these dendritic swellings gave signals slightly below the average, as expected from differences in surface-to-volume ratios (compare spot labelled 'O' with the other 4 dendritic regions).

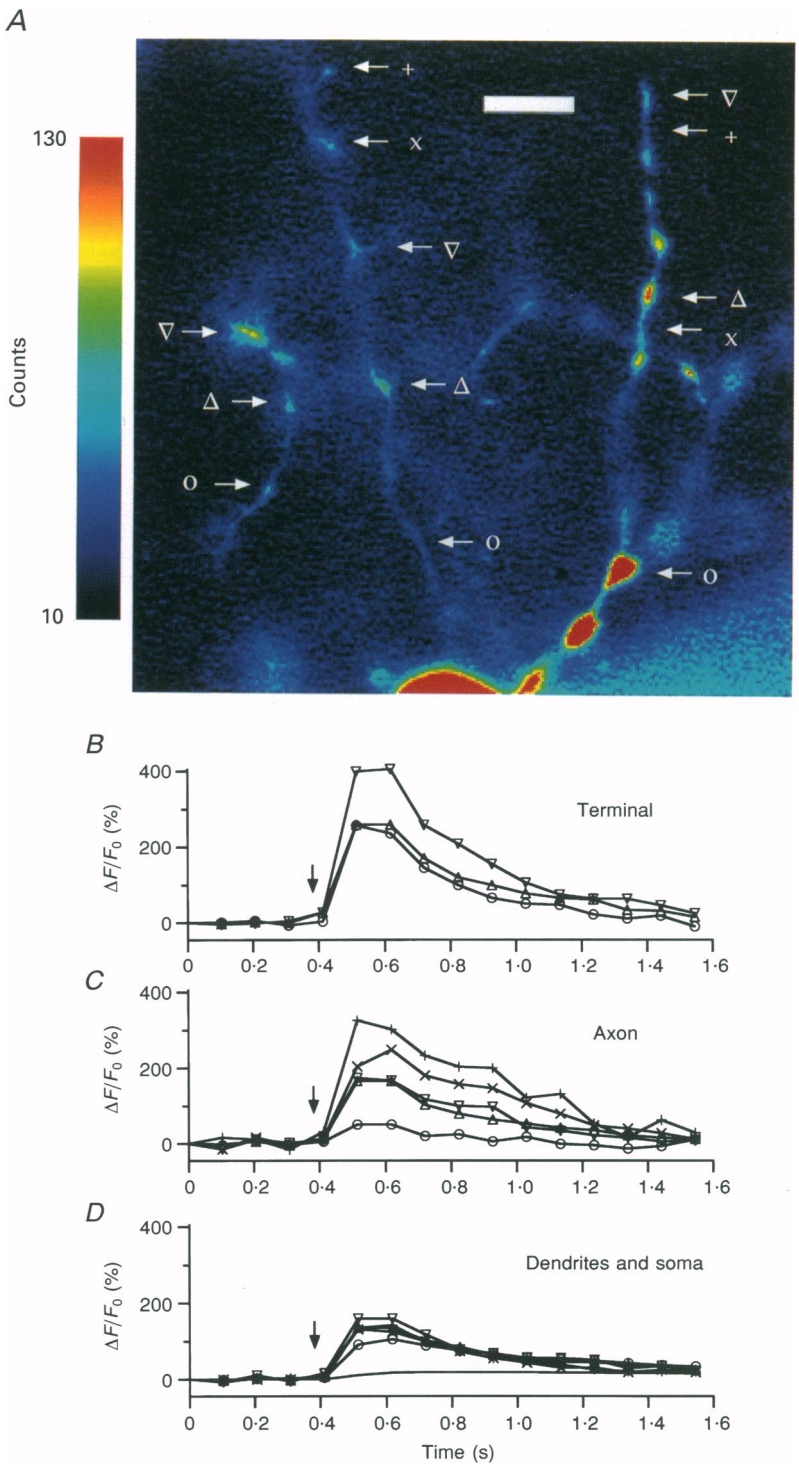

Figure 3. Spatial distribution and time course of depolarization-induced $[Ca^{2+}]_i$ changes in a basket cell

Same experiment as in Fig. 2. Relative changes in fluorescence were measured, as described in Methods, in ROIs identified in *A* by arrows and various symbols. In the left part of the image three regions of interest mark hot spots on a synaptic contact onto the lower Purkinje cell of Fig. 2. In the middle part, 5 ROIs correspond to hot spots (+, ×, ▽, △) or initial segment (○) of the axon. In the right part, 5 ROIs have been selected on one dendrite. Finally, one spot was taken in the soma (continuous line in *D*). The three plots in *B*, *C* and *D* show responses to the depolarizing step (arrows) in the various cell regions as a function of time. The signals are large in synaptic terminals and in axon hot spots, and they are small in the dendrites, in the axon initial segment, and in the soma. Scale bar in *A*, 10 μm.

The situation was drastically different in the axon, which was unambiguously distinguished from the dendrites based on its much larger extension and its orientation parallel to the Purkinje cell layer. Axonal $\Delta F/F_0$ was very heterogeneous (Fig. 3*B* and *C*). Peak values as high as 350% were obtained in spatially restricted regions along the axon and in terminals in contact with Purkinje cells which could be clearly identified, as exemplified by Fig. 2. In contrast to the large transients observed at discrete axonal sites, regions between hot spots had peak $\Delta F/F_0$ of 20–40%. Likewise, there was a long region corresponding to the initial segment of the axon with low $\Delta F/F_0$ (Fig. 3*C*, see also Fig. 4).

A similar spatial pattern of Ca_i^{2+} rises was observed in eleven cells studied. In each cell, one region in the soma centre and five to ten regions in the axon and dendrites were analysed as described in Methods. Peak values of $\Delta F/F_0$ were then averaged for each type of region in a given cell, and the results from the eleven cells were pooled together to provide mean ± S.E.M. values. For 50 ms depolarizing pulses average peak $\Delta F/F_0$ values were 186 ± 19·3% in axonal hot spots (terminals, varicosities and branching points; see below), and 33 ± 7·6% in axonal segments between hot spots and in the proximal axon. The corresponding values were 18·5 ± 3% and 23·9 ± 5·2% in soma and dendrites, respectively. (Note that these numbers are less than those obtained in the experiment of Figs 2 and 3, which used 100 ms pulses.) Although full descriptions of the spatial distribution of Ca_i^{2+} signals in mammalian neurones are not available, the present results are consistent

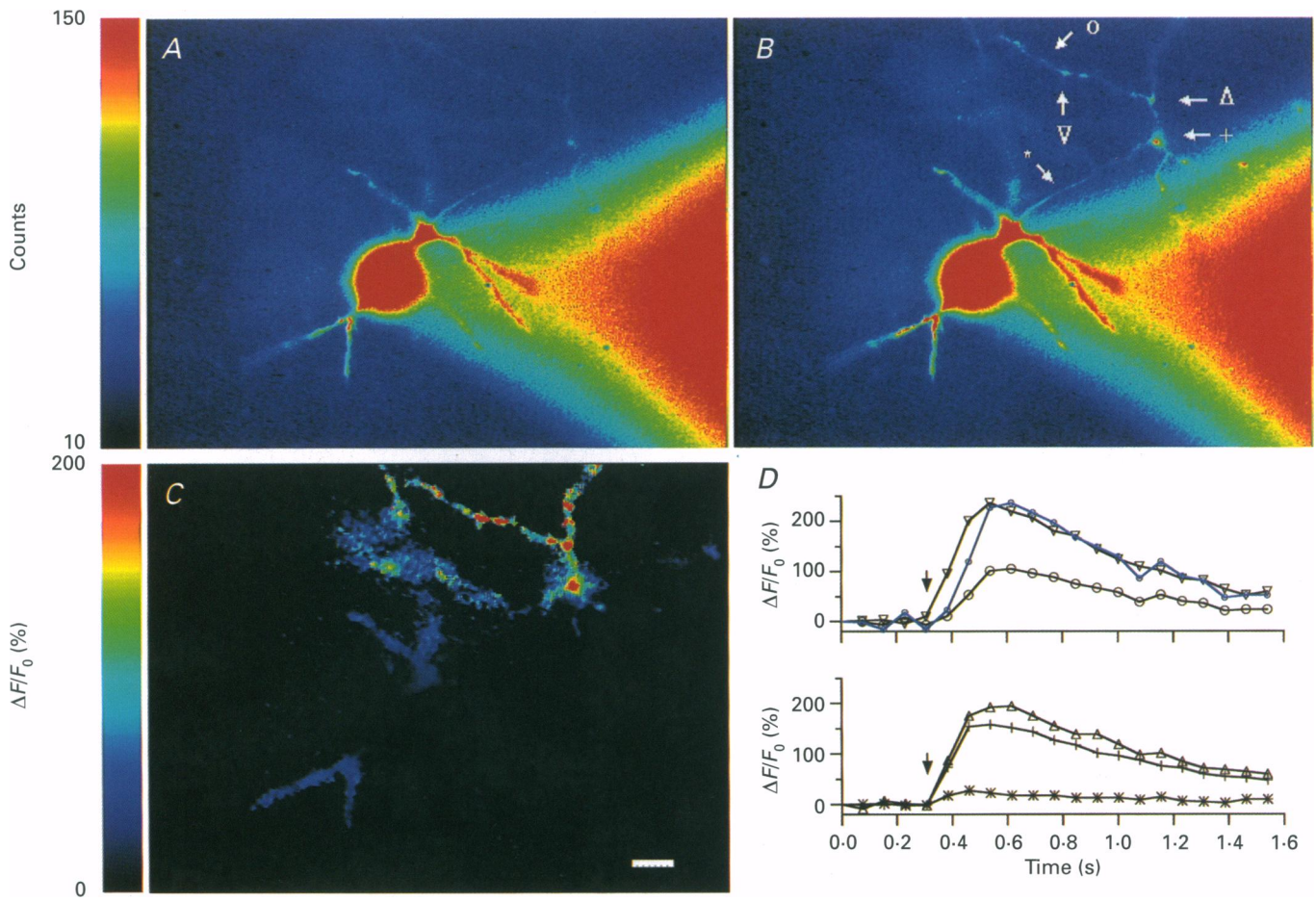

Figure 4. $[Ca^{2+}]_i$ rises in axonal varicosities and branch points

A and *B*, fluorescence images (70 ms exposures) of a basket cell at rest and 51–121 ms after the end of a 100 ms pulse to 0 mV. *C*, $\Delta F/F_0$ image generated from the image shown in *B* and the average of 4 pre-stimulus images; arrows in *B* mark the position of discrete ROIs the analysis of which is displayed in *D*. The lower plot in *D* illustrates hot spots at two branching points of the axon (symbols Δ and +) contrasting with the low amplitude change in fluorescence in the proximal axon (✳). Note in the upper plot in *D* that the ROI in the inter-varicosity region (○) has a smaller amplitude and a slower time course of onset than the neighbouring hot spot (▽); the difference in time course is evident in the trace shown in blue (○) which corresponds to the data from the inter-varicosity ROI scaled to the peak amplitude on the adjacent hot spot. Scale bar in *C*, 10 μm.

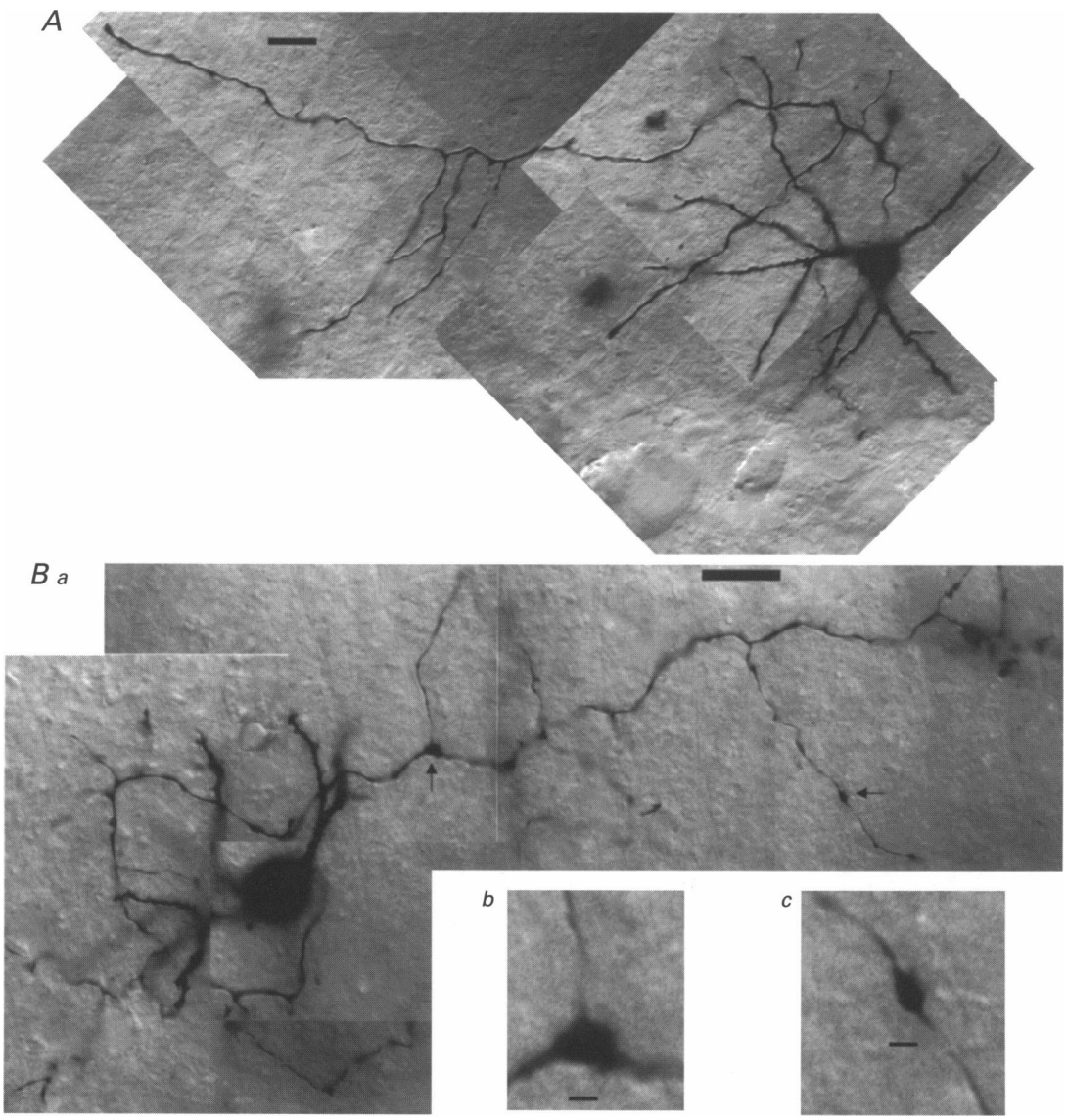

Figure 5. Morphological appearance of biocytin-filled 13-day-old basket cells

A, photomontage of an entire basket cell from photographs taken at ×63 magnification. The Purkinje cell layer is at the bottom of the picture and the pia is at the top. The axon runs towards the pial surface for 20 to 30 μm after its origin (out of focus), it then turns left and its main branch maintains a fairly constant track parallel to the Purkinje cell layer. Along its course the axon gives rise to 6 short ascending collaterals (not longer than 20 μm) and to 5 long descending collaterals (50 μm or more; the first one is partially out of focus). Dendrites have diameters of 0·7–1·0 μm. Scale bar, 10 μm. *Ba*, photomontage of another basket cell from photographs taken at ×100 magnification. As in *A*, the Purkinje cell layer is at the bottom of picture and the pia at the top. Most of the dendrites here are out of focus. The axon origin is on the right of the cell body just below a well-focused dendrite. The axon then makes a hairpin turn around the cell body. During this turn the axon gives rise to several collaterals (the first two are long, branched and reach several Purkinje cells outside the frame). After the end of the turn the axon runs as in *A* at a constant level above the Purkinje cell layer (the end of the axon is out of frame). In this straight portion the main axon again sends off several collaterals. There are prominent variations of the axon diameter at branching points (vertical arrow) and at bouton-like varicosities (horizontal arrow). Scale bar, 10 μm. *b*, enlargement of the branching point indicated by the vertical arrow in *a*. *c*, enlargement of the varicosity indicated by the horizontal arrow in *a*. Scale bar for *b* and *c*, 1 μm.

with partial information from recent studies comparing two subregions at a time. Thus, in the calices of Held, the peak amplitude of CG5N transients evoked by single action potentials is much lower in the proximal axon than in the terminal region (Borst *et al.* 1995). In cortical pyramidal neurones (Schiller, Helmchen & Sakmann, 1995) and in cerebellar Purkinje cells (Callewaert, Eilers & Konnerth, 1996), action potentials evoke Ca_i^{2+} transients of similar magnitudes in proximal dendrites and in the initial portions of the axon, as we find for basket cells.

Axonal hot spots were consistently observed in three cellular domains: (i) terminal portions of the axon contacting a Purkinje cell soma which were often clearly recognisable, as exemplified by Fig. 2, (ii) discrete sites along the axon corresponding to local swellings but with no clear Purkinje cell soma as potential postsynaptic target, and (iii) axonal branching sites. The latter point is illustrated in Fig. 4, where pseudocolour images are shown in control conditions (*A*) and after a 100 ms depolarization (*B*). Two points of axonal branching can be distinguished in the axon of this neurone (marked by △ and + in the image shown in *B*). Both sites experienced large Ca_i^{2+} rises following the depolarizing step. As illustrated by the plots in *D* these depolarization-induced Ca_i^{2+} rises had similar magnitudes and time course to those observed at hot spots along the axon (see ▽ in *D*). The rather unexpected finding of high Ca_i^{2+} rises at axonal branch points was confirmed in all cells studied. Thus, at bifurcation points, peak $\Delta F/F_0$ values for 50 ms pulses were 153 ± 16% (2–4 sites per cell; 9 cells) a value similar to that given above for terminals and varicosities.

Morphological correlates of high local axonal Ca_i^{2+} signals

To obtain insight into the nature of axonal hot spots, images of the axon with long excitation exposures were taken at the end of the recording. Hot spots invariably co-localized with relatively large resting fluorescence signals. These results suggest that hot spots correspond to locally enlarged regions of the axon. Axonal enlargements might reflect swelling due to fluorescence induced cell damage. However, morphological studies in seven basket cells filled with biocytin in recordings without fluorescent dye or strong illumination

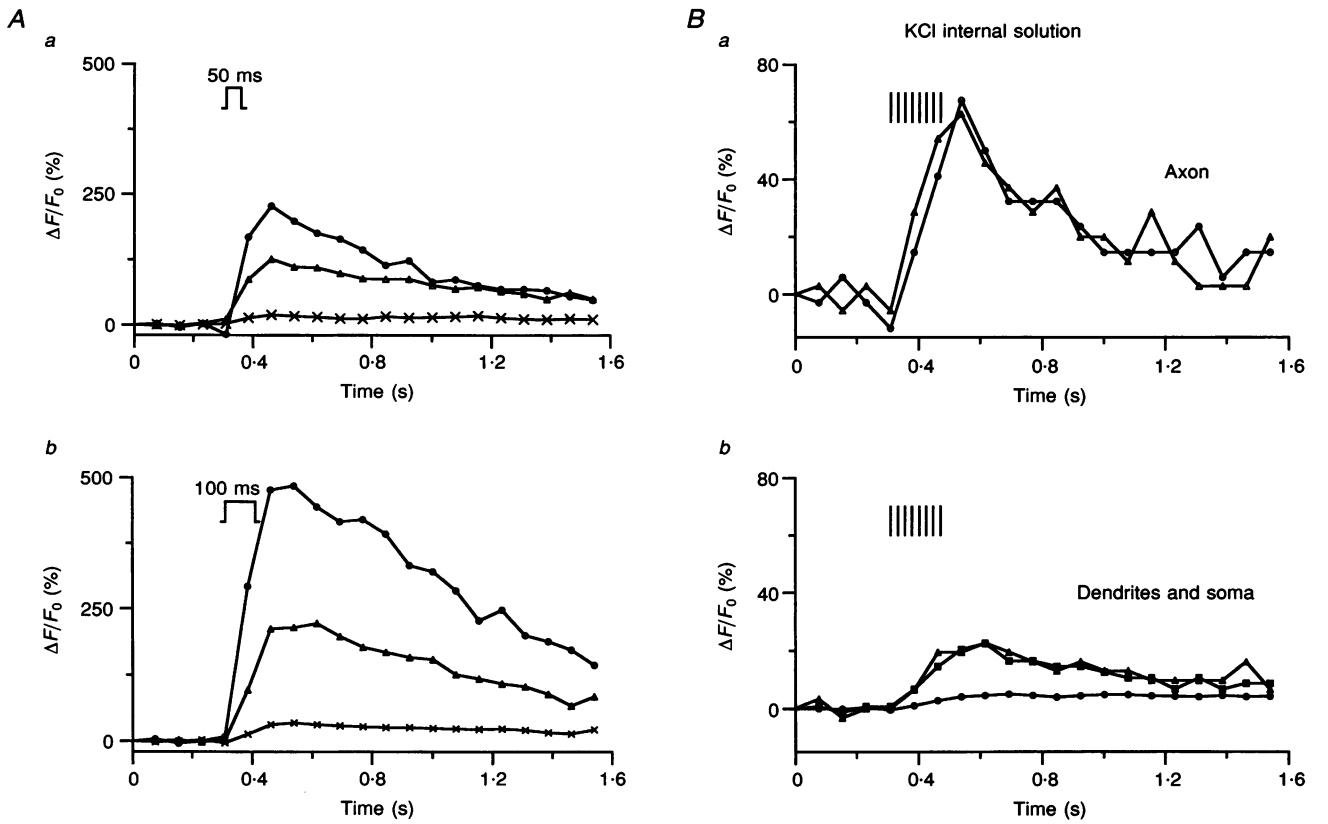

Figure 6. $[Ca^{2+}]_i$ rises under different stimulation conditions

A, modulation of $[Ca^{2+}]_i$ rises by pulse duration. The percentage fluorescence changes for 2 discrete spots in a basket cell axon and 1 spot in its dendrite are related to the duration of the voltage step. Ratios of peak $\Delta F/F_0$ for 100 ms (*Ab*) over 50 ms (*Aa*) are 2·13 and 1·77 for the two axonal spots shown and 1·64 for the dendritic spot. In the soma, the corresponding ratio is 2·38. *B*, $[Ca^{2+}]_i$ rises recorded from a K^+-dialysed basket cell. A train of 8 depolarizing pulses (3 ms duration at 20 ms intervals) leads to changes in fluorescence in 2 axonal spots (*a*) as well as in two dendritic regions and in the soma (*b*). In *A* and *B*, images were acquired with 70 ms exposures.

indicate that this was not the case. Examples of two of these neurones are shown in Fig. 5. The lower power view in Fig. 5*A* illustrates the general appearance of the axon and of the dendritic arborization. In this cell, as well as in that shown at a higher magnification in Fig. 5*Ba*, swellings are present along the main axon, in the collaterals which it sends towards the Purkinje cell layer (Fig. 5*Bc*), in the synaptic terminals onto Purkinje cells, as well as at branching points (Fig. 5*Bb*). Although no published data are available on basket cell morphology at the age window used in the present study, classical Golgi stains by Ramón y Cajal (1911) and by Palay & Chan-Palay (1974) as well as horseradish peroxidase labelling (O'Donoghue *et al.* 1989) have clearly shown that varicosities are a characteristic feature of basket cell axons in adult animals.

Interpretation of high local axonal Ca_i^{2+} signals

As detailed in Methods, conversion of fluorescent signals to $\Delta F/F_0$ ratios effectively eliminates several potential artefacts related to background subtraction, dye distribution and measurement procedures as sources for the spatial heterogeneity in Ca_i^{2+} transients. Other factors which could give rise to this sort of distribution will now be analysed. The first of these factors concerns the surface-to-volume ratio in the different domains. Different surface-to-volume ratios could account for part or all of the difference between Ca_i^{2+} signals in soma and in neurites, but cannot explain the fact that dendrites have much lower signal than axonal hot spots, since these regions have similar diameters. Within the axon, the surface-to-volume ratio is larger in naked regions than in varicosities, branch points or synaptic terminals. Therefore geometrical factors do not account for local heterogeneity in the axonal results. Furthermore, the signals recorded between axonal hot spots were delayed compared with those at neighbouring varicosities (see Fig. 4), suggesting that part or all of the corresponding fluorescence arose from diffusion from hot spots. On the whole the results imply that hot spots correspond to highly elevated local $[Ca^{2+}]_i$ and are a source of Ca^{2+} during the redistribution occurring after depolarizing pulses.

Another potential source of heterogeneity would arise if the depolarization lasts longer in hot spots than elsewhere in the cell, perhaps as a result of loading the cell with Cs^+ ions. Against this possibility we note that the distance between hot spots and intercalated 'cold' stretches of axon is too short to accommodate substantial potential differences. In order to address more directly the question of space clamp control in the axonal arbor, experiments were performed using somatic voltage steps of various duration. Figure 6*A* presents Ca_i^{2+} transients elicited by 50 and 100 ms somatic pulses. One dendritic spot and two axonal varicosities located at less than 60 μm from the soma are analysed. The ratios of peak $\Delta F/F_0$ values for 100 over 50 ms pulses were similar in the dendrite (1·64) and in the two axonal varicosities (2·13 and 1·77). These results suggest that at least some of the hot spots experience voltage changes very similar to those pertaining in the somato-dendritic region, and reinforce the idea that the large Ca_i^{2+} signals at axonal hot spots reflect special features of the local Ca_i^{2+} homeostasis.

As an additional check that the spatial segregation of $[Ca^{2+}]_i$ rises was not an artefact linked to Cs^+ loading we performed experiments with K^+-dialysed basket cells. In these conditions, a short depolarizing pulse evokes a propagated action potential, which leads to evoked IPSCs in paired whole-cell recordings (Vincent & Marty, 1996). Signals following single somatic depolarization were too small (< 4%) to be faithfully analysed. However, clear $[Ca^{2+}]_i$ rises could be elicited with trains of short pulses which mimic the bursting behaviour of basket cells (Eccles *et al.* 1966; Armstrong *et al.* 1979). Although the magnitude of these changes is much smaller than that obtained in Cs^+-loaded cells, the relative amplitude of axonal *versus* dendritic and somatic signals is maintained (Fig. 6*B*). In the axon, these signals had a patchy appearance and decay kinetics similar to those obtained with Cs^+-dialysed cells (time to half-decay, 373 ± 29 ms; 14 cells). The peak value of the $\Delta F/F_0$ transients evoked by eight pulses in axonal hot spots was 39 ± 13% (5 cells).

DISCUSSION

Our results show that following voltage-gated Ca^{2+} entry in a basket cell, $[Ca^{2+}]_i$ rises are very heterogeneous, and are much larger at presynaptic structures and at axonal branch points than elsewhere in the cell. Consideration of Ca^{2+} buffering systems indicates that Ca^{2+} recruitment is even more heterogeneous than the present results suggest. Inhibitory neurones, including basket cells, are known to have high concentrations of Ca^{2+}-binding proteins (reviewed by Baimbridge, Celio & Rogers, 1992). In addition, the concentration of parvalbumin in basket cell axons is 10 times larger than that in the cell soma and dendrites (Kosaka, Kosaka, Nakayama, Hunziker & Heizmann, 1993), suggesting that the endogenous Ca^{2+}-buffering capacity is particularly large in basket cell axons, and that it may be as large as that reported for frog hair saccular cells (Roberts, 1993). Therefore, axonal hot spots are likely to have a much higher density of Ca^{2+} channels (either in the plasma membrane or in intracellular stores) than the somato-dendritic domain. The pattern of Ca_i^{2+} signalling within the axonal domain could arise from (i) non-homogeneous distribution of Ca^{2+} channels or (ii) non-uniformity in Ca^{2+} buffering and/or Ca^{2+} extrusion mechanisms. In the first category, spatial heterogeneity in the density of voltage-gated Ca^{2+} channels in the axonal plasma membrane and/or preferential Ca^{2+}-induced Ca^{2+} release from internal stores at axonal hot spots might be involved. In the second category, non-homogeneities in the distribution of Ca^{2+}-sequestering organelles, Ca^{2+}-binding proteins, pumps, and exchange systems could play a role.

The similarity of signals recorded in axonal swellings and in identified terminals indicates that both sites experience strong $[Ca^{2+}]_i$ rises characteristic of presynaptic specializations and suggests that many of the axonal hot spots are varicosities corresponding to terminals of *en passant* synapses formed by basket cells on dendrites of Purkinje cells and of other interneurones. Ultrastructural studies will be required to determine whether or not presynaptic specializations are also present at axon branch points. Nonetheless, the finding of Ca_i^{2+} hot spots at axonal branch points is of particular interest to signal integration, since Ca_i^{2+} levels regulate the safety factor for propagation of axonal action potentials (Lüscher, Lipp, Lüscher & Niggli, 1996). Thus, $[Ca^{2+}]_i$ rises at branch points could serve to modify the probability of effective transmission to the terminals, particularly during bursts of action potential which are characteristic of basket cells.

From a developmental point of view, it is important to note that although basket cells form synapses onto their target cells quite early in development, ultrastructural changes at synaptic sites occur throughout the first 3 postnatal weeks. Thus, long active zones are present at early stages, and are replaced by shorter, fragmented active zones by postnatal day 21 (Larramendi, 1969). Furthermore, the number of axonal varicosities found in biocytin-filled basket cells at the ages used in the present work is lower than that observed in biocytin fills from adult rats, denoting a maturation process that is accompanied by physiological changes in the strength of synaptic transmission (C. Pouzat & S. Hestrin, personal communication). It will be interesting to investigate if the maturation process involves changes in the properties of axonal Ca_i^{2+} signals.

Although we have not carried out *in situ* calibrations for the conversion of $\Delta F/F_0$ to Ca^{2+} concentration, a rough estimate of $[Ca^{2+}]_i$ may be obtained using *in vitro* calibration curves for CG5N fluorescence as a function of pCa (see Methods). Using a K_d of 20 μM and assuming a resting $[Ca^{2+}]_i$ of 60 nM, the largest $\Delta F/F_0$ obtained at axonal hot spots, in Cs^+-dialysed cells, corresponds to an elevation of $[Ca^{2+}]_i$ to ~1–1·5 μM. Under the more physiological conditions of internal K^+ perfusion, the smaller signals would amount to ~200 nM after a train of eight pulses. The latter estimate is within the range of values reported in various axons of mammalian neurones: for an action potential, estimated $[Ca^{2+}]_i$ changes are ~10–30 nM in hippocampal mossy fibre terminals (Regehr *et al.* 1994; Wu & Saggau, 1994*a*) and in axonal varicosities of cultured cortical neurones (Mackenzie *et al.* 1996); ~50 nM in dorsal root ganglion cells (Lüscher *et al.* 1996); and ~300 nM in cerebellar parallel fibre axons (Regehr & Atluri, 1995). It must be stressed, however, that the Ca_i^{2+} transients measured in the present work as well as in previous studies represent spatial and time averages and do not correspond to the instantaneous local Ca^{2+} transients in the vicinity of the transmitter release sites.

In conclusion, the present report demonstrates the feasibility of a simple approach to measure Ca_i^{2+} signals in single synaptic boutons in brain slices. Sites of contact between basket cell axon terminals and their postsynaptic targets are found at relatively short distances (tens of micrometres) from the basket cell somata, rendering this a promising preparation for further studies on the relation between synaptic transmission (Vincent & Marty, 1996) and Ca_i^{2+} signalling in identified presynaptic terminals.

Armstrong, D. M. & Rawson, J. A. (1979). Activity patterns of cerebellar cortical neurones and climbing fibre afferents in the awake cat. *Journal of Physiology* **289**, 425–448.

Baimbridge, K. G., Celio, M. R. & Rogers, J. H. (1992). Calcium-binding proteins in the nervous system. *Trends in Neurosciences* **15**, 303–308.

Borst, J. G. G., Helmchen, F. & Sakmann, B. (1995). Pre- and postsynaptic whole-cell recordings in the medial nucleus of the trapezoid body of the rat. *Journal of Physiology* **489**, 825–840.

Callewaert, G., Eilers, J. & Konnerth, A. (1996). Axonal calcium entry during fast 'sodium' action potentials in rat cerebellar Purkinje cells. *Journal of Physiology* **495**, 641–647.

Escobar, A. L., Monck, J. R., Fernandez, J. M. & Vergara, J. L. (1994). Localization of the site of Ca^{2+} release at the level of a single sarcomere in skeletal muscle fibres. *Nature* **367**, 739–741.

Llinás, R. & Sasaki, K. (1966). The inhibitory interneurones within the cerebellar cortex. *Experimental Brain Research* **1**, 1–16.

Heidelberger, R., Heinemann, C., Neher, E. & Matthews, G. (1994). Calcium dependence of the rate of exocytosis in a synaptic terminal. *Nature* **371**, 513–515.

Horikawa, K. & Armstrong, W. E. (1988). A versatile mean of intracellular labeling: injection off biocytin and its detection with avidin conjugates. *Journal of Neuroscience Methods* **25**, 1–11.

Haugland, R. P. (1996). *Handbook of Fluorescent Probes and Research Chemicals*, 6th edn. Molecular Probes, Eugene, OR, USA.

Kano, M., Rexhausen, U., Dreessen, J. & Konnerth, A. (1992). Synaptic excitation produces a long-lasting rebound potentiation of inhibitory signals in cerebellar Purkinje cells. *Nature* **356**, 601–604.

Katz, B. & Miledi, R. (1967). A study of synaptic transmission in the absence of nerve impulse. *Journal of Physiology* **192**, 407–436.

Kosaka, T., Kosaka, K., Nakayama, T., Hunziker, W. & Heizmann, C. W. (1993). Axons and axon terminals of cerebellar Purkinje cells and basket cells have higher levels of parvalbumin immunoreactivity than somata and dendrites: quantitative analysis by immunogold labeling. *Experimental Brain Research* **93**, 483–491.

Larramendi, L. M. H. (1969). Analysis of synaptogenesis in the cerebellum of the mouse. In *Neurobiology of Cerebellar Evolution and Development*, ed. Llinás, R., pp. 803–843. American Medical Association, Chicago.

Llano, I. & Gerschenfeld, H. M. (1993). β-Adrenergic enhancement of inhibitory synaptic activity in rat cerebellar stellate and Purkinje cells. *Journal of Physiology* **468**, 201–224.

Llano, I., Leresche, N. & Marty, A. (1991). Calcium entry increases the sensitivity of cerebellar Purkinje cells to applied GABA and decreases inhibitory synaptic currents. *Neuron* **6**, 565–574.

LLANO, I., MARTY, A., ARMSTRONG, C. M. & KONNERTH, A. M. (1991). Synaptic- and agonist-induced excitatory currents of Purkinje cells in rat cerebellar slices. *Journal of Physiology* **434**, 182–213.

LLINÁS, R., SUGIMORI, M. & SILVER, R. B. (1992). Microdomains of high calcium concentration in a presynaptic terminal. *Science* **256**, 677–679.

LÜSCHER, C., LIPP, P., LÜSCHER, H.-R. & NIGGLI, E. (1996). Control of action potential propagation by intracellular Ca^{2+} in cultured rat dorsal root ganglion cells. *Journal of Physiology* **490**, 319–324.

MACKENZIE, P. J., UMEMIYA, M. & MURPHY, T. H. (1996). Ca^{2+} imaging of CNS axons in culture indicates reliable coupling between single action potentials and distal functional release sites. *Neuron* **16**, 783–795.

MESSLER, P., HARZ, H. & UHL, R. (1996). Instrumentation for multiwavelengths excitation imaging. *Journal of Neuroscience Methods* **69**, 1137–1147.

NEHER, E. & AUGUSTINE, G. J. (1992). Calcium gradients and buffers in bovine chromaffin cells. *Journal of Physiology* **450**, 273–301.

O'DONOGHUE, D. L., KING, S. L. & BISHOP, G. A. (1989). Physiological and anatomical studies of the interactions between Purkinje cells and basket cells in the cat's cerebellar cortex: evidence for a unitary relationship. *Journal of Neuroscience* **9**, 2141–2150.

PALAY, S. L. & CHAN-PALAY, V. (1974). *Cerebellar Cortex*. Springer Verlag, New York.

RAMÓN Y CAJAL, S. (1911). Histologie du système nerveux de l'homme et des vertébrés. Maloine, Paris.

REGEHR, W. G. & ATLURI, P. P. (1995). Calcium transients in cerebellar granule cells presynaptic terminals. *Biophysical Journal* **68**, 2156–2170.

REGEHR, W. G., DELANEY, K. R. & TANK, D. W. (1994). The role of presynaptic calcium in short-term enhancement at the hippocampal mossy fiber synapse. *Journal of Neuroscience* **14**, 523–537.

REGEHR, W. G. & TANK, D. W. (1991). The maintenance of LTP at hippocampal mossy fiber synapse is independent of sustained presynaptic calcium. *Neuron* **7**, 451–459.

REGEHR, W. G. & TANK, D. W. (1994). Dendritic calcium dynamics. *Current Biology* **4**, 373–382.

ROBERTS, W. M. (1993). Spatial calcium buffering in saccular hair cells. *Nature* **363**, 74–76.

SCHILLER, J., HELMCHEN, F. & SAKMANN, B. (1995). Spatial profile of dendritic calcium transients evoked by action potentials in rat neocortical neurones. *Journal of Physiology* **487**, 583–600.

SIMON, S. M. & LLINÁS, R. R. (1985). Compartmentalization of the submembrane calcium activity during calcium influx and its significance in transmitter release. *Biophysical Journal* **48**, 485–498.

VINCENT, P., ARMSTRONG, C. M. & MARTY, A. (1992). Inhibitory synaptic currents in rat cerebellar cells: modulation by postsynaptic depolarisation. *Journal of Physiology* **456**, 453–471.

VINCENT, P. & MARTY, A. (1993). Neighboring Purkinje cells communicate via retrograde inhibition of common presynaptic interneurons. *Neuron* **11**, 885–893.

VINCENT, P. & MARTY, A. (1996). Fluctuations of inhibitory postsynaptic currents in Purkinje cells from rat cerebellar slices. *Journal of Physiology* **494**, 183–199.

WU, L. G. & SAGGAU, P. (1994*a*). Presynaptic calcium is increased during normal synaptic transmission and paired-pulse facilitation, but not in long-term potentiation in area CA1 of the hippocampus. *Journal of Neuroscience* **14**, 645–654.

WU, L. G. & SAGGAU, P. (1994*b*). Adenosine inhibits evoked synaptic transmission primarily by reducing presynaptic calcium influx in area CA1 of hippocampus. *Neuron* **12**, 1139–1148.

YUSTE, R. & TANK, D. W. (1996). Dendritic integration in mammalian neurons, a century after Cajal. *Neuron* **16**, 701–716.

ZHAO, M., HOLLINGWORTH, S. & BAYLOR, S. M. (1996). Properties of tri- and tetracarboxylate Ca^{2+} indicators in frog skeletal muscle fibers. *Biophysical Journal* **70**, 896–916.

Acknowledgements

We are grateful to Alain Marty for many helpful discussions throughout the course of this study and to Richard Miles for his comments on the manuscript. We thank Christophe Pouzat for sharing his expertise and data on morphological studies of cerebellar cells. This work was supported by the Max-Planck-Society, grants from the European Community (Copernicus and Capital and Human Mobility programs) and from the Deutsche Forschungsgemeinschaft (SFB 406).

Author's permanent address

C. Caputo: Instituto Venezolano de Investigaciones Científicas, Caracas, Venezuela.

Author's email address

I. Llano: illano@gwdg.de

Received 17 January 1997; accepted 2 May 1997.